Article

Spatio-Temporal Changes in Air Quality of the Urban Area of Chongqing from 2015 to 2021 Based on a Missing-Data-Filled Dataset

Huayu Zhang [1], Yong Nie [1,*], Qian Deng [1,2], Yaqin Liu [1], Qiyuan Lyu [1] and Bo Zhang [1,3]

1 Institute of Mountain Hazards and Environment, Chinese Academy of Sciences, Chengdu 610299, China
2 University of Chinese Academy of Sciences, Beijing 100190, China
3 Faculty of Geosciences and Environmental Engineering, Southwest Jiao Tong University, Chengdu 611756, China
* Correspondence: nieyong@imde.ac.cn

Abstract: Air pollution is one of the severe environmental issues in Chongqing. Many measures made by the government for improving air quality have been put into use these past few years, while the influence of these measures remains unknown. This study analyzed the changes in the air quality of the urban area of Chongqing between 2015 and 2021 using a complete in situ observation dataset that all missing data were filled by the interpolation of a low-rank tensor completion model with truncate nuclear norm minimization (LRTC-TNN). The results include: (1) the LRTC-TNN model robustly performs to reconstruct missing data of pollutant concentrations with an R^2 of 0.93 and an RMSE of 7.78; (2) the air quality index (*AQI*) decreases by 15.96%, and the total polluted days decrease by 21.05% from 2015 to 2021, showing an obvious promotion in air quality; and (3) the changing air quality is attributed to decreasing concentrations of $PM_{2.5}$ (34.10%), PM_{10} (25.03%), and NO_2 (5.53%) from 2015 to 2021, whereas an increasing concentration of O_3 (10.49%) is observed. The processing method for missing data, intact *AQI* datasets, and analysis of changes are beneficial to policy-making for environmental improvement and fill the gap in the field of data interpolation for air quality datasets in mountainous areas.

Keywords: air pollution; *AQI*; environmental protection; missing data interpolation; air pollutant

1. Introduction

Air pollution is one of the severe global environmental issues, which directly affects human health and exacerbates climate change. Studies on the impact of air quality on human health [1–3], human activity decisions [4,5] and environment protection [6–8] caused an increasing focus on the past decades. China was still struggling with grievous air pollution in the past few years, the ambient air quality of 121 out of 339 cities in 2021 exceeded the standard limit [9]. The air quality index (*AQI*) is widely used to measure the level of air quality and is generally calculated by concentrations of six pollutants, including particulate matters ($PM_{2.5}$ and PM_{10}), SO_2, NO_2, O_3, and CO, recorded by an observation network. In 2021, the average concentrations of six pollutants were 30 µg/m³ ($PM_{2.5}$), 54 µg/m³ (PM_{10}), 137 µg/m³ (O_3), 9 µg/m³ (SO_2), 23 µg/m³ (NO_2), and 1.1 mg/m³ (CO) [9]. For example, the concentration of $PM_{2.5}$ was far higher than that of the healthy standard (15 µg/m³) from the World Health Organization (WHO) [10].

Over 3000 observation sites have been built all over China to monitor air quality change for policy-making. The absence of observation data in each site possibly happens as a result of the power cut or malfunction of equipment. An incomplete dataset is likely to lead to a large error in air quality evaluation, which is suggested to be validated and preprocessed before being used [11]. Various methods of data interpolation, such as mean imputation [12], local least-squares fitting [13], and k-nearest neighbors (KNN) [14], were widely used to fill the missing values [15] before analysis. State-of-the-art interpolating

methods include an adaptive radial basis function (RBF) interpolation algorithm by Gao et al. (2020) [16], a multidimensional interpolating based on long short-term memory (LSTM) [17], and a combination of KNN and random forest algorithm (RF-KNN) [18]. The methods mentioned above could consider either the spatial or temporal relationship of data and provide reasonable interpolating solutions, but air quality data are influenced by time and location at the same time, considering that either spatial or temporal characteristics likely results in a large error. Thus, a data interpolation method that combines both spatial and temporal characteristics of data is needed. The tensor completion algorithm is a kind of technique for filling the missing or unobserved entries of partially observed tensors, which has been successfully used in the fields of data mining and data imputation [19]. The low-rank tensor completion (LRTC) showed its advantages in recovering datasets with large missing rates in [20,21]. By carefully constructing the observed tensor, the spatial and temporal characteristics of data can be simultaneously considered, and the accuracy of interpolating results can be improved. Liu et al. (2020) [22] applied an LRTC model to interpolate the missing values for the air pollution time series dataset in Beijing to produce a complete dataset of air quality.

Chongqing is one of the four municipalities with a developed economy and society in China, which has suffered from severe air pollution for many years [4,23]. Rugged mountainous terrain, dense buildings, intense emissions of various pollutants, humid and still air, and increasing population [24,25] are known to be the contributors to air pollution. Since the 13th 5-year plan for the development of ecology and environment was proposed, many measurements and policies, such as factory renovation and the promotion of electrical vehicles, have been made to improve the air quality [26]. However, few research studies emphasize the spatial and temporal changes in air quality and the concentration of related pollutants in Chongqing after measures and policies of environmental protection have been made for years.

This study aims to (1) produce a complete dataset of air quality by filling the missing values of site observation data in Chongqing using an advanced LRTC model, (2) reveal the latest spatial and temporal variation of air quality from 2015 to 2021 based on the reconstructed dataset, and (3) interpret the causes of air quality changes and implication for eco-environmental protection in the mountainous area.

2. Study Area

The main urban area of Chongqing is selected as the study area limited by the availability of observation sites (Figure 1a), covering nine counties with a total area of 5472 km^2. Chongqing (105°17′–110°11′ N, 28°10′–32°13′ E) is a typical mountainous city with an elevation between 100 and 2796 m above sea level [27], where the Daba Mountains, Wu Mountains, Wuling Mountains, and Dalou Mountains are situated to the north, east, southeast, and south of Chongqing, respectively, and Yangtze and Jialing Rivers flow across the main cities from the west to the east [28]. Chongqing is dominated by a four-season humid subtropical climate with an air temperature usually spanning from 6 to 35 °C and annual precipitation ranging from 1000 to 1400 mm annually [27]. In 2021, Chongqing had a gross domestic product (GDP) of CNY 2.80 trillion, approximately 5 million private vehicles, and a total population of 32 million, including a population of 22 million in the main urban area [29].
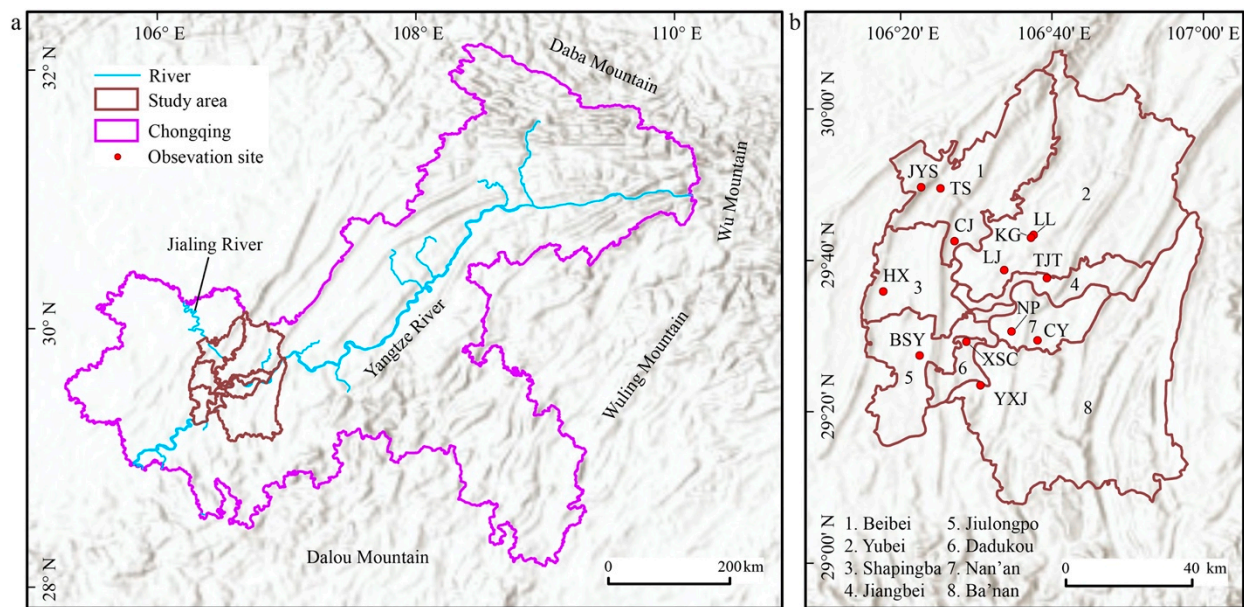
Figure 1. Location of the study area in Chongqing (**a**) and distribution of observation sites (red dots) in related counties (**b**).

3. Data and Methodology

3.1. Data

A total of 61,320 h of observation of 13 sites spanning from 2 January 2015 to 31 December 2021 was collected for air quality analysis in the study area between 2015 and 2021, downloaded from the China Environment Monitoring Terminal (http://www.cnemc.cn/ (accessed on 10 March 2022)). The 13 observation sites are distributed within eight counties (Figure 1b), of which five counties have one observation site, respectively, one county has two observation sites, and two counties have three observation sites. Additionally, data recorded from four sites named 1415A, 1423A, 1424A, and 1430A are excluded from the study area due to the suspension of recording since November 2016. The raw data of each site contain the hourly record of *AQI* and six major pollutants ($PM_{2.5}$, PM_{10}, SO_2, NO_2, O_3, and CO). The missing rates of raw data vary among 13 observation sites (Table S1) with a mean missing rate of 4.80%, the highest missing rate of 5.93% at site 1428A, and the lowest missing rate of 4.21% at site 1426A.

3.2. Methodology

3.2.1. AQI Calculation

AQI is a comprehensive index of six pollution factor subindices that are generally calculated based on the technical regulation of the Ministry of Ecology and Environment [30]. To determine the hourly and daily *AQI*, the individual air quality index (*IAQI*) of each pollutant needs to be first calculated based on the value of each pollutant, and then the maximum value is taken as the *AQI*. Hourly *AQI* is directly calculated based on the original hourly record, and daily *AQI* is calculated based on the daily (24 h) average values of PM_{10}, $PM_{2.5}$, SO_2, NO_2, CO mass concentration, and the daily maximum 8 h sliding average of O_3 mass concentration. Monthly, seasonal, and annual AQIs are calculated by averaging the daily *AQI* of the responding period. The formula for calculating *AQI* can be expressed as:

$$\mathrm{AQI}_i = \frac{C_{i,m} - C_{i,j-1}}{C_{i,j} - C_{i,j-1}} \times \left(\mathrm{AQI}_{i,j} - \mathrm{AQI}_{i,j-1} \right) + \mathrm{AQI}_{i,j-1}$$
$$\mathrm{AQI} = \max(AQI_1, AQI_2, AQI_3 \dots, AQI_i)$$

(1)

where AQI_i is the *IAQI* of a pollutant item, $C_{i,m}$ is the mass concentration value of the pollutant item, $C_{i,j}$ and is the pollutant close to $C_{i,m}$. The high value of the concentration

limit, $C_{i,j-1}$, is the low value of the pollutant concentration limit close to $C_{i,m}$; $AQI_{i,j}$ is the corresponding individual air quality index to $C_{i,j}$; and $AQI_{i,j-1}$ is the individual air quality index corresponding to $C_{i,j-1}$. When calculating the hourly and daily *AQI*, the concentrations of PM_{10}, $PM_{2.5}$, SO_2, NO_2, CO, and O_3 need to be calculated after segmenting them according to the breakpoints in Table S2.

3.2.2. Missing Values Interpolation

LRTC with truncate nuclear norm (TNN) minimization (LRTC-TNN) [31] was used to interpolate the missing values of air quality data. According to the principle of tensors, the lower the rank of a tensor is, the stronger the relationship of data in a tensor will be. Therefore, interpolating missing values in a dataset can be converted into recovering a tensor when the rank of this tensor is low. TNN is defined as the summation of the minimum singular values of $min\{m,n\} - r$ when a matrix $X \in \mathbb{R}^{m*n}$ and a positive integer $r < min\{m,n\}$ are given [32].

In this study, a third-order tensor (*sites* $\times$ *days* $\times$ *hours*) was constructed for the tensor completion. A third-order LRTC-TNN model [31] can be expressed as:

$$\min_{\mathcal{X}} \sum_{k=1}^{3} \propto_k \| x_{k(k)} \|_{r_k,*}$$
$$s.t. \ p_\Omega(\mathcal{M}) = p_\Omega(\mathcal{Y}) \tag{2}$$

With the truncate for each tensor mode being:

$$r_k = \left\lceil \theta * \min\left\{n_k, \prod_{h \neq k} n_h\right\} \right\rceil, \forall k \in \{1,2,3\} \tag{3}$$

For notions [31,33,34], $\mathcal{X} \in \mathbb{R}^{m \times n \times t}$ denotes the target tensor that is assumed to be found; $\mathcal{Y} \in \mathbb{R}^{m \times n \times t}$ denotes the observed tensor; $\| \mathcal{X} \|_{r,*}$ denotes the TNN of a given third-order tensor $\mathcal{X}$; $\propto_1$, $\propto_2$, and $\propto_3$ ($\sum_k \propto_k = 1$) denote the weight parameters imposed on the TNN of unfolding matrices, respectively; Ω is the index of the observed entries; and operation $p_\Omega : \mathbb{R}^{m \times n \times t} \to \mathbb{R}^{m \times n \times t}$ is an orthogonal projection supported on Ω:

$$[p_\Omega(\mathcal{X})]_{mnt} = f(x) = \begin{cases} x_{mnt}, & if \ (m,n,t) \in \ \Omega, \\ 0, & otherwise, \end{cases} \tag{4}$$

For any tensor $\mathcal{X}$, the operator $p_\Omega^\perp : \mathbb{R}^{m \times n \times t} \to \mathbb{R}^{m \times n \times t}$ denotes the projection onto the complementary set of Ω. The relationship between these two operators is: $p_\Omega(\mathcal{X}) + p_\Omega^\perp(\mathcal{X}) = \mathcal{X}$. $\lceil . \rceil$ denotes the smallest integer value that is no less than the given value, θ is a universal rate parameter that controls the whole truncation on three modes of $\mathcal{X}$. It should satisfy $1 \leq r_k < min\left\{n_k, \prod_{h \neq k} n_h\right\}$.

In this study, an optimized algorithm called the alternating direction method of multipliers (ADMM) was used to determine the tensor $\mathcal{X}$ [35]. By defining global rate parameters, the algorithm automatically determines the given data of the tensor nuclear norm of each mode truncation to control the degree of truncation. As an optimized algorithm, ADMM decomposes the original problem into serval solvable subproblems and obtains the optimized solution by coordinating the solution of each subproblem. To determine the tensor $\mathcal{X}$ by using ADMM, the LRTC-TNN model [31] can be expressed as:

$$\mathcal{L}\left(\mathcal{M}, \{x_k, \gamma_k\}_{k=1}^3\right) = \sum_{k=1}^{3} (\alpha_k \| x_{(k)} \|_{r_k,*} + \frac{\rho_k}{2} \| x_{k(k)} - \mathcal{M}_k \|_F^2 + \langle x_k - \mathcal{X}, \gamma_k \rangle) \ \forall k \in \{1,2,3\} \tag{5}$$

where $\langle .,. \rangle$ denotes the inner product, $\| \bullet_F \|$ denotes the Frobenius norm, ρ denotes the learning rate, and $\gamma_k \in \mathbb{R}^{m \times n \times t}$ are used for a dual update in the following ADMM scheme. This model can be converted into the following three subproblems [31] iteratively:

$$x_k^{l+1} := \arg \min_x \mathcal{L}\left(\mathcal{M}, \left\{ x_k^{l+1}, \gamma_k^l \right\}_{k=1}^3 \right) \tag{6}$$

$$\mathcal{M}^{l+1} := \arg \min_M \mathcal{L}\left(\mathcal{M}, \left\{ x_k^{l+1}, \gamma_k^l \right\}_{k=1}^3 \right) \tag{7}$$

$$\gamma_k^{l+1} := \gamma_k^l + \rho_k \left(x_k^{l+1} - \mathcal{M}^{l+1} \right) \tag{8}$$

Updating x_k^{l+1}, $\mathcal{M}^{l+1}$, and γ_k^{l+1} once can finalize one iteration of matrix completion, and the target tensor $\mathcal{X}$ is found when the ADMM runs to convergence.

The LRTC-TNN model was used to interpolate the missing values of six pollutants in the raw dataset; then hourly and daily AQIs were calculated based on Equation (1) using a complete dataset that all missing values of the six pollutants were filled. To validate the robustness of interpolating, we took the observation site 1414A (JYS) as an example, randomly removed 5% of the values of the six pollutants with a reference to its original missing rate, and compared the observed *AQI* and interpolation-calculated *AQI*. The statistics showed that the interpolated *AQI* calculated with the interpolated values of the six pollutants matched well with the originally observed *AQI* with an R^2 of 0.93 and a root mean square error (RMSE) of 7.78 (Figure 2), and the LRTC-TNN model was suitable for interpolating the missing value of air quality data.
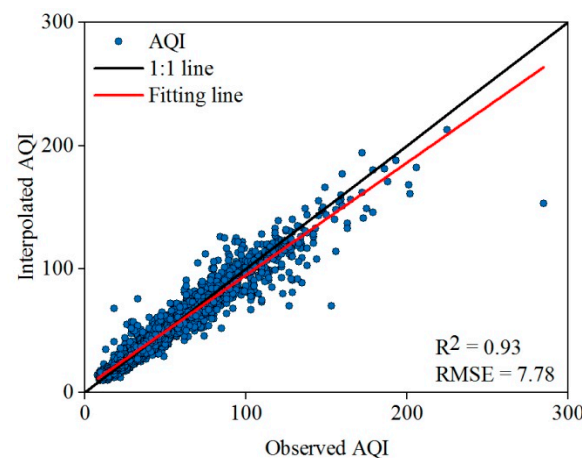

Figure 2. Comparison between observed hourly *AQI* and interpolated hourly *AQI*.

3.2.3. Spatial and Temporal Analysis of AQI

Based on the hourly and daily AQIs, a group of time series plots was used to depict the temporal variation. A generalized additive model entitled natural cubic splines was adopted to create a fitting line [36], reflecting the variation of *AQI* over time. The monthly, seasonal, and annual changes in *AQI* and the change in days of annual primary pollutants were similarly described as the hourly and daily changes in *AQI*.

The spatial variation derived from the air quality data of 13 observation sites between 2015 and 2021 in the study area was analyzed. The air quality of each county was represented by the arithmetic mean value of the *AQI* of the observation sites that were within this county. Subsequently, the spatial variation in days of the primary pollutants was shown.

Air quality is categorized into six classes based on the *AQI* (Table S3). Primary pollutants refer to the pollution item with the largest *IAQI* value in an hour or 1 day. A day is regarded as a polluted day when the *AQI* of a day is greater than 100.

4. Result

4.1. Distribution Characteristics of AQI

The overall air quality in the main urban area of Chongqing was at the level of good with a mean, median, and standard deviation of 63, 56, and 36, respectively, for the hourly *AQI* observed from 2015 to 2021. The recorded maximum and minimum hourly AQIs were 500 and 6, respectively (Table S4).The spatial heterogeneity of *AQI* among 13 observation sites was relatively low, and a boxplot distribution of *AQI* at each observation site was similar (Figure S1). The mean *AQI* ranged from 49 to 68, and the median *AQI* spanned from 45 to 60 for most observation sites. The observation site XSC had the highest mean (68), median (60), and standard deviation (39), whereas the observation site JYS had the lowest mean (49), median (45), and standard deviation (28). The observation site LJ had the largest range from 6 to 500 in contrast to the observation site JYS with the smallest range from 7 to 285 (Table S4).

4.2. Temporal Variation Analysis

4.2.1. Hourly Variation

The time series of hourly *AQI* at all observation sites showed a decreasing trend from 2015 to 2021 (Figure 3). The fitting line of hourly *AQI* exhibited a similar decreasing trend with slightly various magnitudes for observation sites except for the JYS site. The *AQI* of most observation sites decreased obviously from 2015 to 2016, then increased from 2016 to 2017, continued to fall to the bottom in 2020, and finally rebounded from 2020 to 2021. The anomalous site (JYS in Beibei) showed a relatively flat declining trend from 2015 to 2021. The JYS site had the lowest hourly *AQI* in 2015 (mostly lower than 100) in contrast to other sites with many values greater than 100 in 2015 and presented a rapidly decreasing trend from 2015 to 2016.

A decreasing trend was also observed in the 24 h mean *AQI* from 2015 to 2021 (Figure S2). The *AQI* value of the night (18:00 to 6:00) was higher than that of the day (6:00 to 18:00) from 2015 to 2019; however, the difference between the night and the day was not significant during 2020–2021. The hourly mean AQIs from 20:00 to 2:00 in 2015 (mean *AQI* value of 85) and from 21:00 to 1:00 in 2016 (mean *AQI* value of 84) were higher than those of other periods. The hourly mean *AQI* from 5:00–7:00 in 2020 was the lowest from 2015 to 2021 with a mean value of 50.

4.2.2. Daily Variation

The time series of daily *AQI* showed a similarly changing trend as that of hourly *AQI*, and the decreasing trend of daily *AQI* was smoother than that of hourly *AQI* (Figure 4). The daily *AQI* at the observation site JYS nearly showed a relatively flat downward trend, while the daily *AQI* of other observation sites showed a fluctuating decreasing trend from 2015 to 2021, including a dramatic decline from 2015 to 2016.

4.2.3. Monthly, Seasonal, and Annual Changes

Monthly *AQI* showed a periodical change from January to December ((Figure 5a), presenting a nearly w-shaped fluctuation that a high *AQI* appeared in January–February, July–August, and December, and a low *AQI* came in March–June and September–November. The mean monthly *AQI* was 102 in January (highest) and 58 in October (lowest). The maximum monthly *AQI* was recorded in January 2015 (value of 157) in contrast with the minimum monthly *AQI* of 51 in October 2019. The changing trend of monthly *AQI* differed from 2015 to 2021. An upward trend was observed in June.

A seasonal change in *AQI* (Figure 5b) was clear from spring to winter from 2015 to 2021, presenting an increase of 8.33% from spring to summer, a decrease of 17.94% from summer to fall, and an increase of 35.94% from fall to winter. The mean seasonal *AQI* was 87 for winter (highest), 78 for summer, 72 for spring, and 64 for fall (lowest). The maximum seasonal *AQI* appeared in the winter of 2016 (value of 102) in contrast with the minimum of 57 in the fall of 2020. The changing trend of seasonal *AQI* differed from 2015 to 2021. A

relatively stable trend was observed in summer, while the other three seasons showed a consistent decreasing trend. The decreasing rate was 1.52% for fall, 8.70 for winter, and 22.78% for spring.
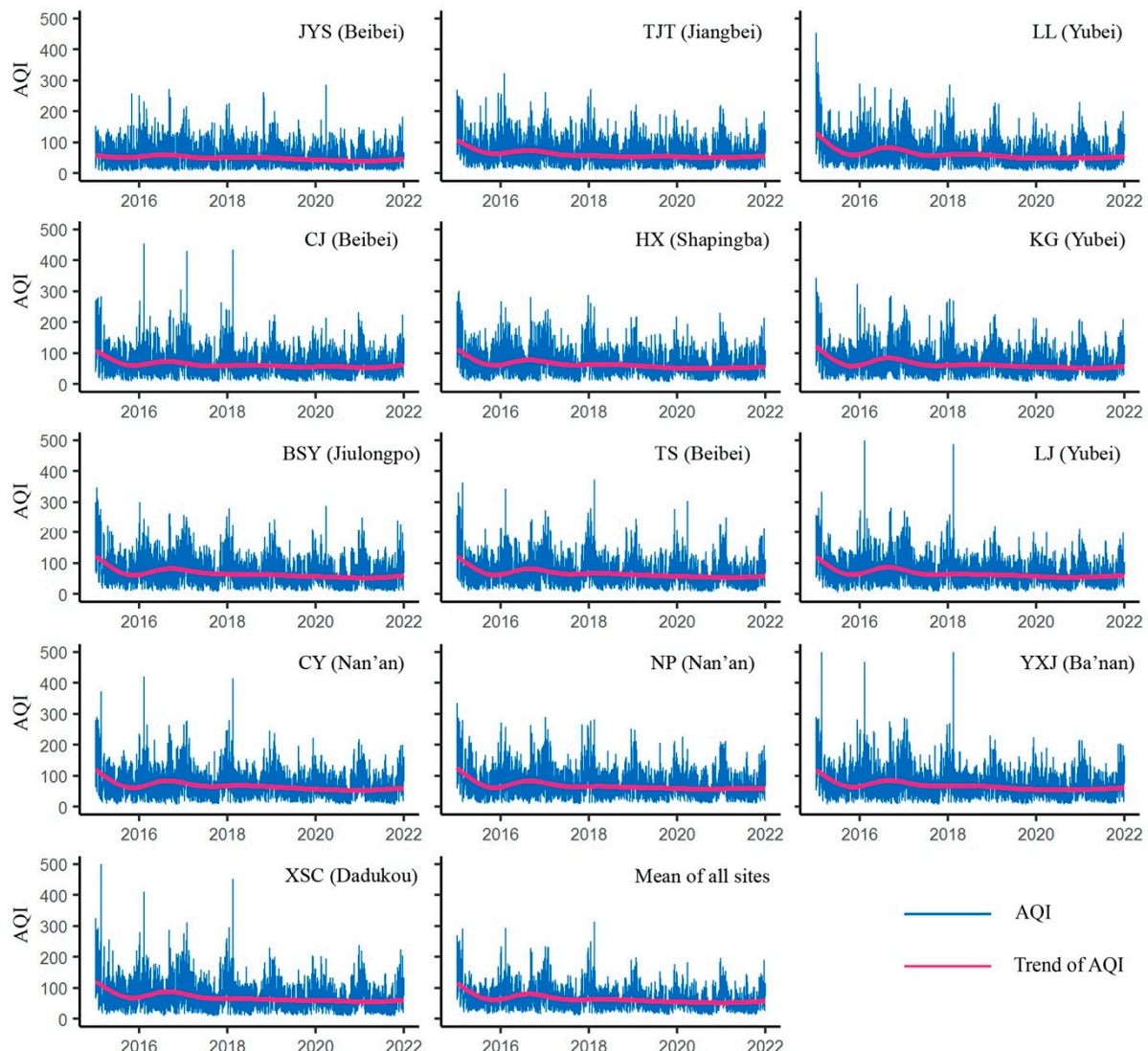

Figure 3. Time series changes of hourly *AQI* for each site and mean of all sites between 2015 and 2021.

The annual *AQI* in the whole study area witnessed a continuously declined trend from 2015 to 2020 and then rebounded in 2021 ((Figure 5c). The maximum annual *AQI* appeared in 2015 (value of 83) in contrast with a minimum value in 2020 (value of 68). An interannual changing trend of annual *AQI* varied from 2015 to 2021. The overall decreasing rate from 2015 to 2021 was 15.96% and 2.66% per year. The maximum interannual decreasing rate (8.15%) of yearly *AQI* appeared during 2017–2018. Annual *AQI* remained stable during 2016–2017 and increased by 3.04% during 2020–2021.

4.2.4. Contributors to Daily Air Pollution

A total of 506 of 2556 days were recorded to be polluted (AQI greater than 100) from 2015 to 2021 (Table S5), and the primary pollutant of 289 days was from $PM_{2.5}$, 212 days from O_3, 4 days from NO_2, and 1 day from PM_{10}. The annual total of polluted days increased from 76 days in 2015 to 97 days in 2017, then fell to 43 days in 2020, and finally rebounded to 60 days in 2021 (Table S5). Correspondently, the air quality of the main urban area of Chongqing was becoming better from 2015 to 2021. In addition, the primary

pollutants were mainly $PM_{2.5}$ and O_3, and the proportion of the different contributing rates of major primary pollutants varied from 2015 to 2021. The days of $PM_{2.5}$ as a primary pollutant occupied 80.23% in 2015 and decreased to 55.00% in 2021. The days of O_3 as a primary pollutant took up 19.74% in 2015 and increased to 45.00% in 2021.
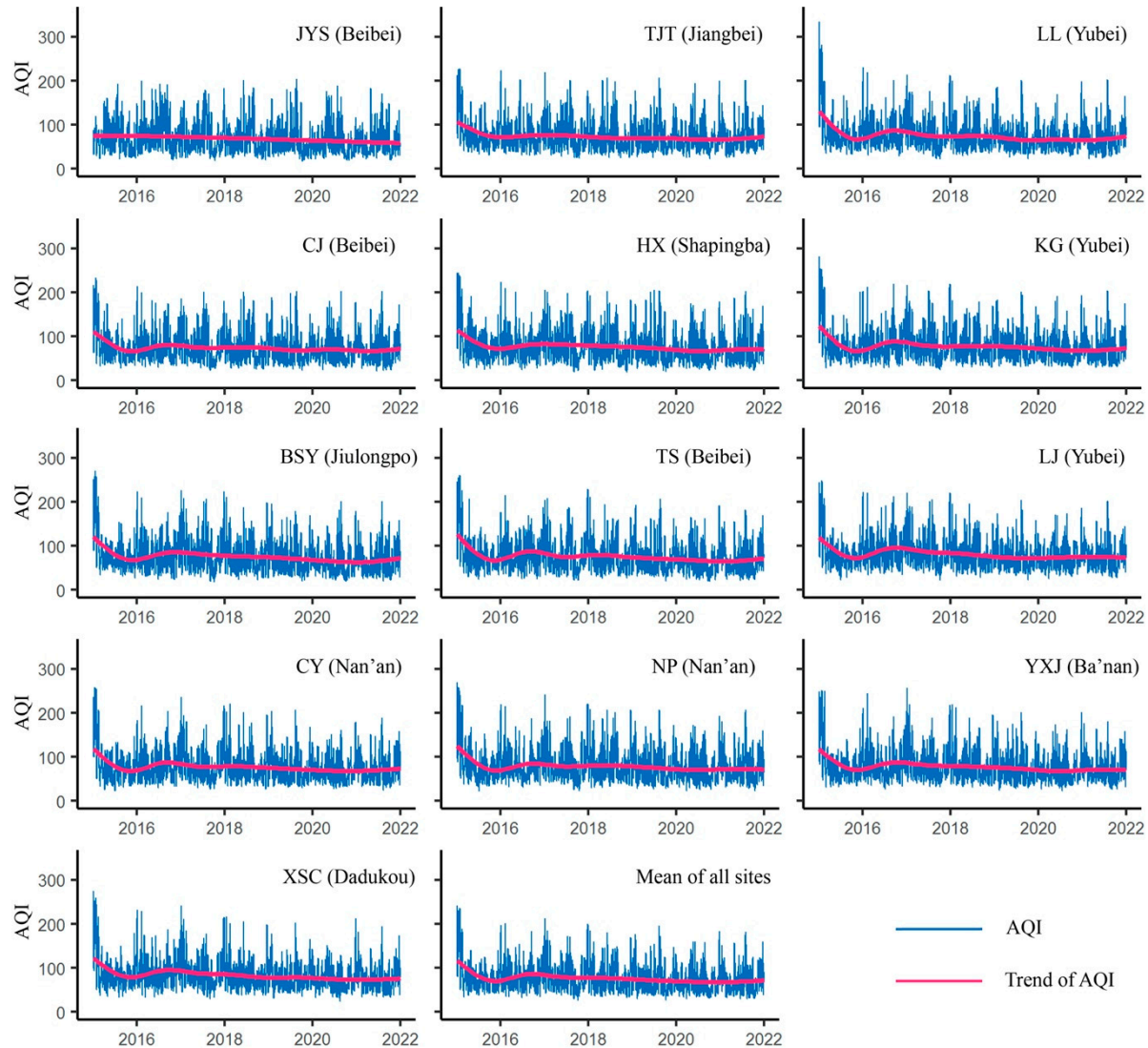

Figure 4. Time series changes of daily *AQI* for each site and mean of all sites between 2015 and 2021.

The proportion in order of severity of air pollution varied from 2015 to 2021 (Figure 6). The days that were unhealthy for sensitive groups took up the largest portion of the polluted days in all 7 years, and its proportion increased from 60.52% in 2015 to 86.05% in 2021. The days that were unhealthy occupied the second largest part of polluted days, and it declined from 26.32% in 2015 to 15.00% in 2021. The days that were very unhealthy were the smallest part of polluted days, and it was only recorded from 2015 to 2017. No hazardous days were recorded from 2015 to 2021.

4.3. Spatial Heterogeneity of AQI Changes
4.3.1. Monthly Spatial Variation

The spatial heterogeneity could be seen in the spatial variation of monthly *AQI* (Figure 7). The monthly *AQI* of Dadukou was highest in most months, and the highest *AQI* of Dadukou could be observed in January (value of 111). The monthly *AQI* of Beibei was usually lower than that of other counties, and the lowest monthly *AQI* of this

county could be found in October (value of 51). The monthly *AQI* of the other six counties showed a similar trend, ranging from 55 to 110 during a year.
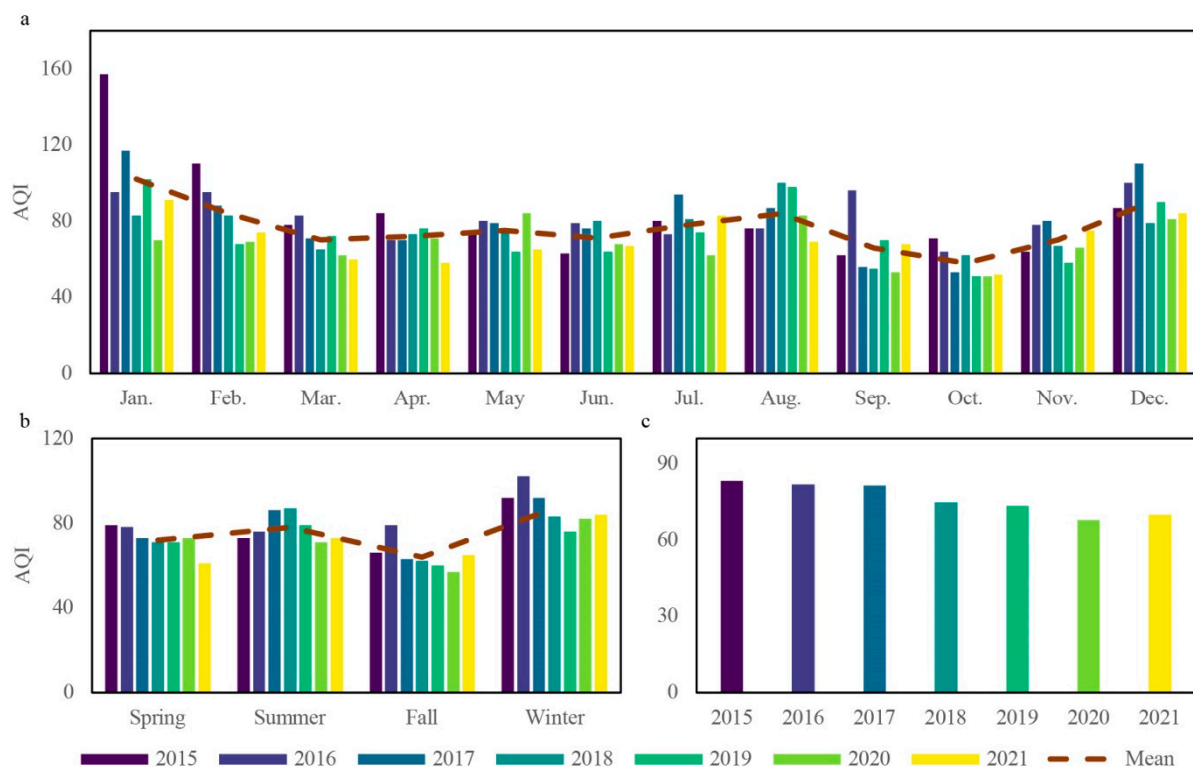

Figure 5. Temporal variation of *AQI* on the scale of months (**a**), seasons (**b**), and years (**c**).
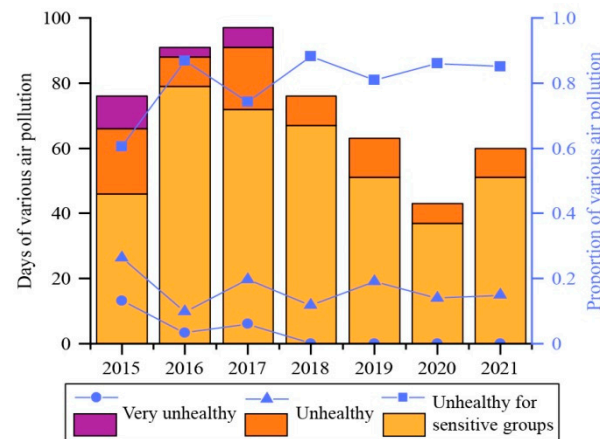

Figure 6. Annual days and proportions of various severity of air pollution from 2015 to 2021.

4.3.2. Seasonal Spatial Variation

The spatial heterogeneity of seasonal *AQI* was clear (Figure S3). The *AQI* of the spring of Dadukou (value of 81) was the highest among eight counties; in contrast, the *AQI* of the spring of Beibei, Jiulongpo, and Jiangbei was lower than that of other counties (values of 69, 69, and 69, respectively). The *AQI* of the summer of Beibei was the highest (value of 81) among eight counties, while the other eight counties had similar *AQI* ranging from 75 to 79, and the lowest *AQI* of the summer could be seen in Ba'nan (value of 75). The highest *AQI* of the fall could be found in Dadukou (value of 75), compared with the lowest *AQI* of the fall in Beibei (value of 59), and the *AQI* of the fall in other counties spanned from 61 to 67. The *AQI* of the winter of Dadukou was the highest (value of 94) while that of Beibei was the lowest (value of 76), and the other six counties had the *AQI* of the spring ranging from 84 to 88.
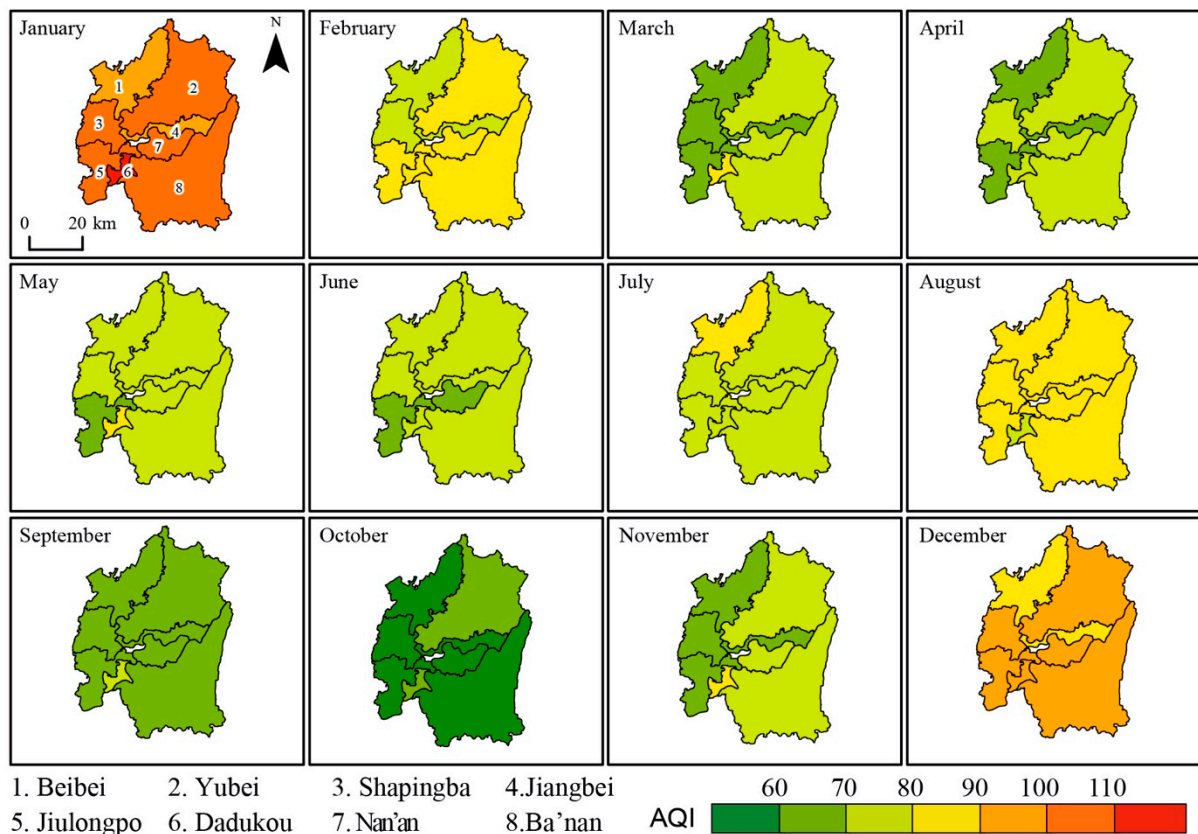
Figure 7. Spatial heterogeneity of monthly *AQI* from 2015 to 2021.

4.3.3. Annual Spatial Variation

The spatial heterogeneity still existed in annual *AQI* (Figure 8a). The annual *AQI* of Dadukou was higher than that of other counties from 2015 to 2021 and reached its peak (value of 91) in 2016. The annual *AQI* of Beibei was usually the lowest except in 2016 and 2018 and reached its bottom (values of 66) in 2020. The annual *AQI* of the other six counties displayed similar changes, and the annual *AQI* ranged from 68 to 85. Remarkably, the annual *AQI* of all counties decreased from 2015 to 2021, showing a great improvement in air quality.

4.3.4. Contributors of Spatial Changes of *AQI*

The polluted days and corresponding primary pollutants showed spatial heterogeneity from 2015 to 2021 (Figure 8b). Dadukou had the most polluted days compared with those other counties in the 7 years and reached its peak (113 days) in 2016. The primary pollutants of Dadukou mainly consisted of $PM_{2.5}$, O_3, and NO_2, $PM_{2.5}$ occupied the largest proportion of primary pollutants of the total polluted days (54.47%), followed by O_3 (26.64%), NO_2 (18.55%), and other pollutants (0.44%). Jiangbei was the county that had the lowest polluted days from 2015 to 2021 and reached its bottom (37 days) in 2020. The primary pollutants of Jiangbei mainly included $PM_{2.5}$ and O_3, and these two pollutants took up 50.38% and 48.88% of the total polluted days, respectively, and other pollutants took up 0.74%. The polluted days showed a downtrend from 2015 to 2021, indicating that the air quality was becoming better.
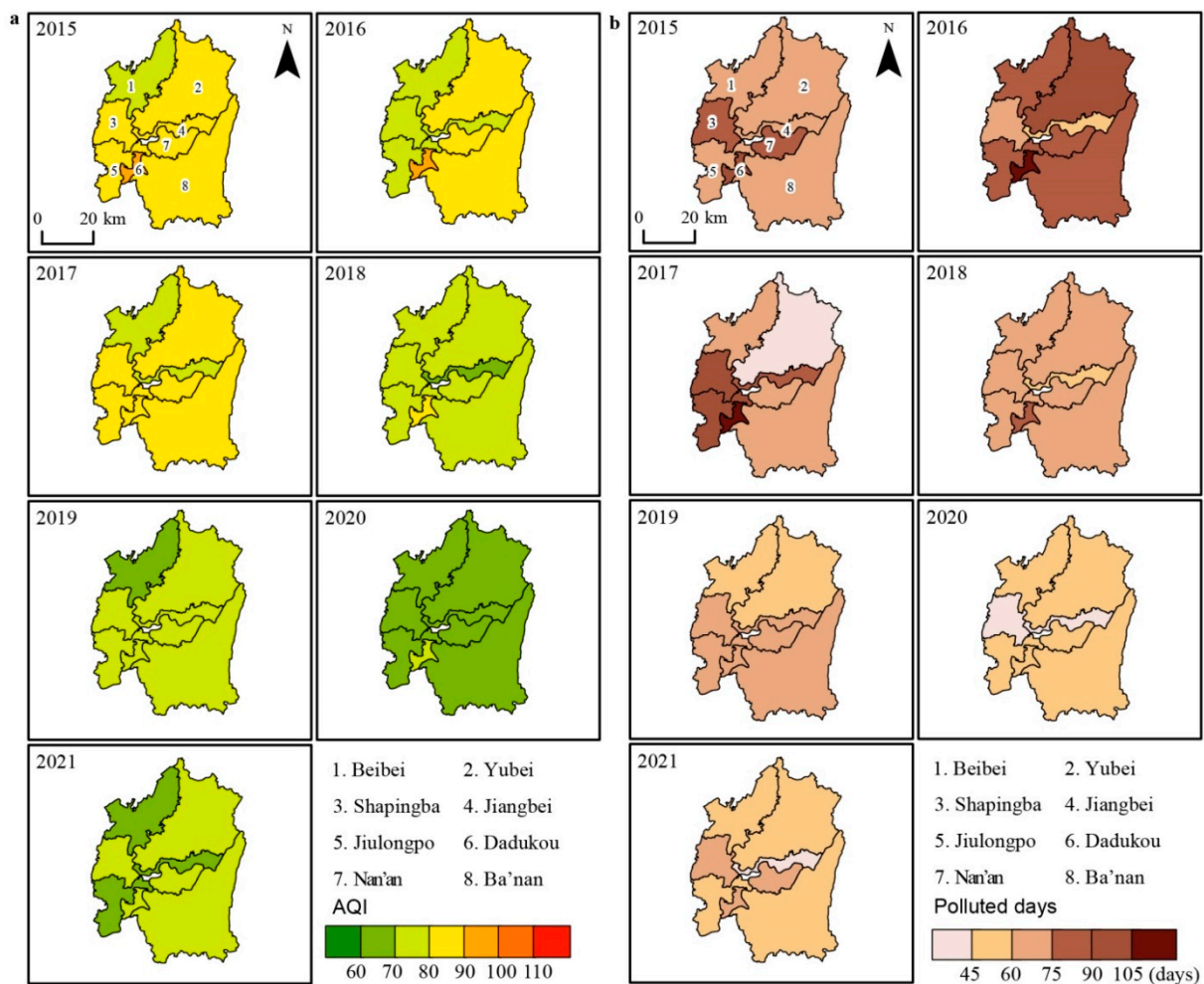
Figure 8. Spatial heterogeneity of annual *AQI* (**a**) and polluted days (**b**) from 2015 to 2021.

5. Discussion

5.1. Driving Factors for AQI Change in Chongqing during 2015–2021

The *AQI* of the main urban area of Chongqing showed an overall downward trend on the scales of hours, days, months, and years, and the polluted days decreased by 21.05% from 2015 to 2021. This is in line with the conclusion by Fan et al. (2020) [37], implying that the air quality of Chongqing was experiencing a great improvement from 2015 to 2021. Considering an *AQI* that is controlled by the maximum values of six pollutants, the reduction of *AQI* indicates a decrease in the concentration of six the pollutants. The concentration of the primary pollutants decreased by 34.10% for $PM_{2.5}$, 5.53% for NO_2, and 25.03% for PM_{10} from 2015 to 2021, while the concentration of O_3 increased by 10.49% (Figure 9).

Industrial consumption and emission are the major sources of pollutants, and the upgrading of industry and energy consumption plays a dominant role in reducing the concentration of pollutants. The backward production capacity has been eliminated in key industries, such as steel, cement, and electrolytic aluminum. From 2016 to 2020, the total energy consumption was 88.75 million tons of standard coal, the cumulative reduction of energy consumption per unit of GDP was 19.4%, the cumulative reduction of carbon dioxide emissions per unit of GDP was 23%, and the proportion of coal consumption dropped to 44.3%, which was 12.5% lower than the national average. The proportion of the secondary industry, including main polluting industries, decreased from 27.8% in 2015 to 25.1% in 2020 [26,38].
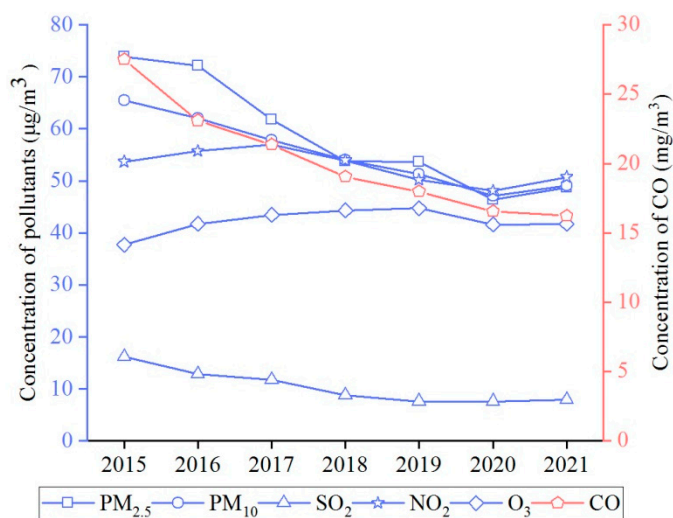
Figure 9. Temporal trend of pollutants including $PM_{2.5}$, PM_{10}, O_3, SO_2, NO_2 (blue), and CO (red) from 2015 to 2021.

Automobile exhaust is another main source of air pollutants, and it is confined by the following reasons. First, the passing of related standards and policies, such as limits and measurement methods for emissions from light-duty vehicles (CHINA 6), effectively reduces automobile exhaust [39]. Although the number of automobiles in Chongqing increased from 5.67 million in 2017 to 7.65 million in 2020, pollutants exhausted from automobiles, including nitrogen oxide (NOx), and particulate matter diminished from 163,100 tons in 2017 to 89,600 tons in 2020 [29,40,41]. Second, the development of public transportation contributes to the reduction of automobile exhaust [42,43]. From 2016 to 2020, 168 km of subway lines was built, and another 16 subway lines with a total length of about 200 km are under construction. The average daily passenger flow of public transportation increased from 1.73 million to 3.09 million. The share of rail transit trips in central urban areas increased from 12.4% to 18.1%. The proportion of total public transit trips increased from 20.4% to 33.0% [44]. Third, the rise of new energy vehicles helps reduce automobile exhaust as well [45]. By the end of 2021, there were approximately 130,000 electric vehicles in Chongqing, accounting for 2.72% of the total vehicles [46]. The decreasing *AQI* on all three time scales from 2015 to 2021 shows a positive response of air quality to shifting environmental protection policies.

Remarkably, the concentration of O_3 increased while the concentration of other pollutants decreased from 2015 to 2021. The increasing concentration of O_3 is likely owing to increasing emissions of volatile organic compounds (VOCs) that have been partially converted into O_3 via reacting with solar radiation [47]. This conversion process is related to the decreasing concentration of particulate matter that causes an increasing amount of solar radiation to reach the land surface and react with VOCs to produce more O_3 [37,48].

Although the *AQI* on three time scales of the main urban area of Chongqing is overall decreasing, it still shows a periodical change. The highest monthly *AQI* is always in winter corresponding to December, January, and February, and the lowest in fall corresponding to September, October, and November. Fan et al. (2020) [37] stated that the concentration of particulate matter is always high in winter, while the concentration of O_3 is high in summer. It indicates that the primary pollutant of winter is dominated by particulate matter, and the primary pollutant of summer is dominated by O_3. A high concentration of particulate matter in winter results from low wind speed, precipitation, and relative humidity, which are controlled by the meteorological conditions of winter in Chongqing [49].

Both the annual polluted days and the mean *AQI* of 2020 are the lowest from 2015 to 2021. This phenomenon is also shown in the time series of hourly and daily AQIs, especially for the first 4 months of 2020. This is owing to the nationwide lockdown of the ongoing COVID-19 (SARS-CoV-2) pandemic from 23 January 2020 to 8 April 2020. This lockdown

leads to the closure of most enterprises, and citizens are not allowed to perform outdoor activities. According to Chen et al. (2020) [50], the concentrations of pollutants including PM2.5, PM10, and NOx decreased by 30%–50% during the COVID-19 lockdown, implying that the air quality could be improved by reducing human-activity-induced emission of pollutants.

5.2. Causes for the Spatial Heterogeneity of AQI

The spatial heterogeneity of *AQI* in the main urban area of Chongqing has been observed at the scales of months, seasons, and years, possibly caused by the variability in population density and distance between the observation site and the pollutant emission source. On all three different scales, the *AQI* of Dadukou is usually the highest, while the *AQI* of Beibei is the lowest. This is likely attributed to the various population densities in different regions [51,52]. According to the Bureau of Statistics of Chongqing (2020) [29], the population density in 2019 was 4032 per km^2 in Dadukou and 1090 per km^2 in Beibei associated with the annual *AQI* of 79 in Dadukou and 70 in Beibei, showing that a higher population density leads to a higher *AQI*. Similarly, the population densities of Shapingba and Nan'an in 2019 were 3675 and 4486 per km^2, respectively, and the annual AQIs of these two counties in 2019 were 74 and 75, respectively.

AQI level is closely related to the environmental setting of its observation site and its distance to the pollutant emission source zone. For example, the air quality at the site 1414A located in Jinyunshan, which is a national nature reserve, is better than that of observation sites in nonprotected areas, such as the site 1417A in Yubei. In addition, the observation sites 1422A and 1428A are near parks, where vegetation cover fractions are high. The recorded *AQI* in these two observation sites is also relatively lower than that of other sites that are surrounded by less fraction of vegetation cover. According to the Bureau of Ecology and Environment of Chongqing (2020) [40], 88 polluting enterprises in Ba'nan exhausted flue gas of approximately 22 billion m^3 in 2020, which was far higher than the average flue gas of the main urban area of Chongqing (17.5 billion m^3) in 2020. The air quality of Ba'nan was supposed to be severe based on the fact of high emission of flue gas, but the *AQI* of Ba'nan on all three different scales was at a relatively medium level among eight counties from 2015 to 2021. This possibly relates to the distance between observation sites and polluting sources. The straight-line distance between the observation site (1429A) and the economic industrial parks of Ba'nan is over 10 km, which exceeds the valid monitoring range from 500 to 4000 m for most observation sites [53]. All those indicate that the location of observation sites plays a critical role in the spatial heterogeneity of air quality.

5.3. Novelty and Limitation

This study utilized a novel method (LRTC-TNN) to fill the missing value in a dataset of air quality. Compared with traditional tensor completion algorithms that consider all singular values, the LRTC-TNN model only focuses on the smallest singular values, which helps the algorithm run more effectively [31,54,55]. Compared with interpolating methods that only consider either temporal or spatial relationships among data [22,56,57], the LRTC-TNN model simultaneously combines the spatial and temporal relationship among data and shows a robust result (R^2 of 0.93 and RMSE of 7.78) in this study.

Limitations in the spatiotemporal analysis of *AQI* in Chongqing are inevitable from limited observation sites, low availability of related data, and running efficiency of the interpolating algorithm. First, using the sparse observation sites in each county to represent the whole county is likely to result in uncertainty at the county scale, and analysis based on more observation sites enhances the representativeness at the county scale. Second, distinguishing the contribution ratio of *AQI* changes from social and physical factors is still a challenge for us due to the lack of firsthand socioeconomic data and related analysis model, these shortcomings are scheduled to be improved in the next step of research. Third, tensor completion algorithms are a kind of time-consuming algorithm, especially when the

processing dataset is large. A more efficient optimization algorithm, such as logarithmic norm regularized tensor factorization [58], is scheduled to improve the effectiveness and make a comparative analysis in the future.

6. Conclusions

This study presents up-to-date spatiotemporal changes in *AQI* and air quality in the main urban area of Chongqing using a complete dataset reconstructed by a novel method (LRTC-TNN) for interpolating missing values. The main findings are as follows:

The randomly selected samples validates the robustness of an interpolating method with high accuracy (R^2 of 0.93 and RMSE of 7.78).

AQI shows an overall downward trend from 2015 to 2021 in the study area. The lowest *AQI* was recorded in 2020 because of the nationwide lockdown for the ongoing COVID-19 pandemic. *AQI* shows periodical change with years and seasons; the highest *AQI* appears in the winter and the lowest occurs in the fall. The spatial heterogeneity of *AQI* changes is obvious; for example, the *AQI* of Dadukou and Nan'an is higher than that of the other counties. This spatial heterogeneity is attributed to the difference in population densities, the number of enterprises, and so on among different counties.

The primary pollutants of daily *AQI* are $PM_{2.5}$ and O_3. The polluted days of all categories shows a downward trend from 2015 to 2021, in which days that are very unhealthy for people have vanished since 2018. The polluted days also shows a spatial heterogeneity, Dadukou had the most polluted days among all counties, and Jiangbei had the lowest polluted days compared with that of other counties. The decrease in *AQI* is primarily attributes to the upgrading of industry and energy consumption and the reduction of automobile exhaust.

Supplementary Materials: The following supporting information can be downloaded at: https://www.mdpi.com/article/10.3390/atmos13091473/s1, Figure S1: A boxplot of hourly *AQI* for each site from 2015 to 2021; Figure S2: Heatmap of 24 h mean *AQI* from 2015 to 2021; Figure S3: Spatial heterogeneity of seasonal *AQI* from 2015 to 2021; Table S1: Overview of observation sites; Table S2: Concentration breakpoints of pollutant items; Table S3: Categories of air quality; Table S4: Descriptive statistics of each observation site from 2015 to 2021; Table S5: Primary contributors of polluted days in Chongqing from 2015 to 2021.

Author Contributions: Conceptualization, H.Z. and Y.N.; methodology, H.Z., Y.L. and Y.N.; software, H.Z., Y.L. and Q.L.; validation, Q.D., Y.N. and B.Z.; data curation, H.Z.; writing—original draft preparation, H.Z. and Y.N.; writing—review and editing, H.Z., Y.N., Q.D., Y.L., Q.L. and B.Z.; visualization, H.Z. and Q.D.; supervision, Y.N.; project administration, Y.N.; funding acquisition, Y.N. All authors have read and agreed to the published version of the manuscript.

Institutional Review Board Statement: Not applicable.

Informed Consent Statement: Not applicable.

Data Availability Statement: The dataset is available on reasonable request from the corresponding author.

Conflicts of Interest: The authors declare no conflict of interest.

References

1. Sarkodie, S.A.; Owusu, P.A. Global Effect of City-to-City Air Pollution, Health Conditions, Climatic & Socio-Economic Factors on COVID-19 Pandemic. *Sci. Total Environ.* **2021**, *778*, 146394. [CrossRef] [PubMed]
2. Pan, R.; Wang, X.; Yi, W.; Wei, Q.; Gao, J.; Xu, Z.; Duan, J.; He, Y.; Tang, C.; Liu, X.; et al. Interactions between Climate Factors and Air Quality Index for Improved Childhood Asthma Self-Management. *Sci. Total Environ.* **2020**, *723*, 137804. [CrossRef] [PubMed]
3. Gorai, A.K.; Tchounwou, P.B.; Biswal, S.; Tuluri, F. Spatio-Temporal Variation of Particulate Matter(PM2.5) Concentrations and Its Health Impacts in a Mega City, Delhi in India. Environ. *Health Insights* **2018**, *12*, 1178630218792861. [CrossRef]

4. Liu, X.; Zhao, C.; Niu, J.; Su, F.; Yao, D.; Xu, F.; Yan, J.; Shen, X.; Jin, T. Spatiotemporal Patterns and Regional Transport of Ground-Level Ozone in Major Urban Agglomerations in China. *Atmosphere* **2022**, *13*, 301. [CrossRef]
5. Benchrif, A.; Wheida, A.; Tahri, M.; Shubbar, R.M.; Biswas, B. Air Quality during Three Covid-19 Lockdown Phases: *AQI*, PM2.5 and NO$_2$ Assessment in Cities with More than 1 Million Inhabitants. *Sustain. Cities Soc.* **2021**, *74*, 103170. [CrossRef] [PubMed]
6. Chen, L.-W.A.; Chien, L.-C.; Li, Y.; Lin, G. Nonuniform Impacts of COVID-19 Lockdown on Air Quality over the United States. *Sci. Total Environ.* **2020**, *745*, 141105. [CrossRef]
7. Xu, H.; Yan, C.; Fu, Q.; Xiao, K.; Yu, Y.; Han, D.; Wang, W.; Cheng, J. Possible Environmental Effects on the Spread of COVID-19 in China. *Sci. Total Environ.* **2020**, *731*, 139211. [CrossRef]
8. Subhanullah, M.; Ullah, S.; Javed, M.F.; Ullah, R.; Akbar, T.A.; Ullah, W.; Baig, S.A.; Aziz, M.; Mohamed, A.; Sajjad, R.U. Assessment and Impacts of Air Pollution from Brick Kilns on Public Health in Northern Pakistan. *Atmosphere* **2022**, *13*, 1231. [CrossRef]
9. Ministry of Ecology and Environment of the People's Republic of China. *Report on the State of the Ecology and Environment in China 2021*; Ministry of Ecology and Environment of the People's Republic of China: Beijing, China, 2022.
10. World Health Organization. *WHO Global Air Quality Guidelines: Particulate Matter (PM2.5 and PM10), Ozone, Nitrogen Dioxide, Sulfur Dioxide and Carbon Monoxide*; World Health Organization: Geneva, Switzerland, 2021; ISBN 978-92-4-003422-8.
11. García, S.; Ramírez-Gallego, S.; Luengo, J.; Benítez, J.M.; Herrera, F. Big Data Preprocessing: Methods and Prospects. *Big Data Anal.* **2016**, *1*, 9. [CrossRef]
12. Noor, M.N.; Yahaya, A.S.; Ramli, N.A.; Al Bakri, A.M.M. Mean Imputation Techniques for Filling the Missing Observations in Air Pollution Dataset. *Key Eng. Mater.* **2013**, *594–595*, 902–908.
13. Chang, G.; Zhang, Y.; Yao, D. Missing Data Imputation for Traffic Flow Based on Improved Local Least Squares. *Tsinghua Sci. Technol.* **2012**, *17*, 304–309. [CrossRef]
14. Park, S.-H.; Bang, S.-W.; Jhun, M.-S. On the Use of Sequential Adaptive Nearest Neighbors for Missing Value Imputation. *Korean J. Appl. Stat.* **2011**, *24*, 1249–1257. [CrossRef]
15. Luengo, J.; García, S.; Herrera, F. On the Choice of the Best Imputation Methods for Missing Values Considering Three Groups of Classification Methods. *Knowl. Inf. Syst.* **2012**, *32*, 77–108. [CrossRef]
16. Gao, K.; Mei, G.; Cuomo, S.; Piccialli, F.; Xu, N. Adaptive RBF Interpolation for Estimating Missing Values in Geographical Data. In Proceedings of the International Conference on Numerical Computations, Crotone, Italy, 15–21 June 2019; Volume 11973, pp. 122–130.
17. Song, W.; Gao, C.; Zhao, Y.; Zhao, Y. A Time Series Data Filling Method Based on LSTM—Taking the Stem Moisture as an Example. *Sensors* **2020**, *20*, 5045. [CrossRef] [PubMed]
18. Zhang, X.; Gui, K.; Liao, T.; Li, Y.; Wang, X.; Zhang, X.; Ning, H.; Liu, W.; Xu, J. Three-Dimensional Spatiotemporal Evolution of Wildfire-Induced Smoke Aerosols: A Case Study from Liangshan, Southwest China. *Sci. Total Environ.* **2021**, *762*, 144586. [CrossRef] [PubMed]
19. Song, Q.; Ge, H.; Caverlee, J.; Hu, X. Tensor Completion Algorithms in Big Data Analytics. *ACM Trans. Knowl. Discov. Data* **2019**, *13*, 6:1–6:48. [CrossRef]
20. Chu, D.; Shen, H.; Guan, X.; Chen, J.M.; Li, X.; Li, J.; Zhang, L. Long Time-Series NDVI Reconstruction in Cloud-Prone Regions via Spatio-Temporal Tensor Completion. *Remote Sens. Environ.* **2021**, *264*, 112632. [CrossRef]
21. Cao, F.; Cai, M.; Tan, Y. Image Interpolation via Low-Rank Matrix Completion and Recovery. *IEEE Trans. Circuits Syst. Video Technol.* **2015**, *25*, 1261–1270. [CrossRef]
22. Liu, X.; Wang, X.; Zou, L.; Xia, J.; Pang, W. Spatial Imputation for Air Pollutants Data Sets via Low Rank Matrix Completion Algorithm. *Environ. Int.* **2020**, *139*, 105713. [CrossRef]
23. Gao, H.; Yang, W.; Wang, J.; Zheng, X. Analysis of the Effectiveness of Air Pollution Control Policies Based on Historical Evaluation and Deep Learning Forecast: A Case Study of Chengdu-Chongqing Region in China. *Sustainability* **2021**, *13*, 206. [CrossRef]
24. Chen, Y.; Xie, S.; Luo, B.; Zhai, C. Particulate Pollution in Urban Chongqing of Southwest China: Historical Trends of Variation, Chemical Characteristics and Source Apportionment. *Sci. Total Environ.* **2017**, *584–585*, 523–534. [CrossRef]
25. Liu, Y.; Yue, W.; Fan, P.; Zhang, Z.; Huang, J. Assessing the Urban Environmental Quality of Mountainous Cities: A Case Study in Chongqing, China. *Ecol. Indic.* **2017**, *81*, 132–145. [CrossRef]
26. Bureau of Ecology and Environment of Chongqing. 14th Five-Year Plan for Ecological Environmental Protection in Chongqing (2021–2025). Available online: http://sthjj.cq.gov.cn/zwgk_249/zfxxgkzl/fdzdgknr/ghjh/202202/t20220216_10400261_wap.html (accessed on 11 July 2022).
27. Zhan, Z.-Z.; Liu, H.-B.; Li, H.-M.; Wu, W.; Zhong, B. The Relationship between NDVI and Terrain Factors—A Case Study of Chongqing. *Procedia Environ. Sci.* **2012**, *12*, 765–771. [CrossRef]
28. Li, W.; Wang, Y.; Xie, S.; Cheng, X. Coupling Coordination Analysis and Spatiotemporal Heterogeneity between Urbanization and Ecosystem Health in Chongqing Municipality, China. *Sci. Total Environ.* **2021**, *791*, 148311. [CrossRef]
29. Bureau of Statistics of Chongqing. Chongqing Statistical Yearbook 2021. Available online: http://tjj.cq.gov.cn/zwgk_233/tjnj/tjnj.html?url=http://tjj.cq.gov.cn/zwgk_233/tjnj/2021/indexch.htm (accessed on 12 July 2022).
30. Ministry of Ecology and Environment of the People's Republic of China. *Technical Regulation on Ambient Air Quality Index (AQI) (on Trial)::HJ 633-2012[S] 2012*; Ministry of Ecology and Environment of the People's Republic of China: Beijing, China, 2012.

31. Chen, X.; Yang, J.; Sun, L. A Nonconvex Low-Rank Tensor Completion Model for Spatiotemporal Traffic Data Imputation. *Transp. Res. Part C Emerg. Technol.* **2020**, *117*, 102673. [CrossRef]

32. Zhang, D.; Hu, Y.; Ye, J.; Li, X.; He, X. Matrix Completion by Truncated Nuclear Norm Regularization. In Proceedings of the 2012 IEEE Conference on Computer Vision and Pattern Recognition, Providence, RI, USA, 16–21 June 2012; pp. 2192–2199.

33. Liu, J.; Musialski, P.; Wonka, P.; Ye, J. Tensor Completion for Estimating Missing Values in Visual Data. *IEEE Trans. Pattern Anal. Mach. Intell.* **2013**, *35*, 208–220. [CrossRef]

34. Kolda, T.G.; Bader, B.W. Tensor Decompositions and Applications. *SIAM Rev.* **2009**, *51*, 455–500. [CrossRef]

35. Hu, Y.; Zhang, D.; Ye, J.; Li, X.; He, X. Fast and Accurate Matrix Completion via Truncated Nuclear Norm Regularization. *IEEE Trans. Pattern Anal. Mach. Intell.* **2013**, *35*, 2117–2130. [CrossRef]

36. Zhao, C.; Sun, Y.; Zhong, Y.; Xu, S.; Liang, Y.; Liu, S.; He, X.; Zhu, J.; Shibamoto, T.; He, M. Spatio-Temporal Analysis of Urban Air Pollutants throughout China during 2014–2019. Air Qual. Atmos. *Health* **2021**, *14*, 1619–1632. [CrossRef]

37. Fan, H.; Zhao, C.; Yang, Y. A Comprehensive Analysis of the Spatio-Temporal Variation of Urban Air Pollution in China during 2014–2018. *Atmos. Environ.* **2020**, *220*, 117066. [CrossRef]

38. Chongqing Development and Reform Commission. 14th Five-Year Plan for Energy Development of Chongqing (2021–2025). Available online: http://www.cq.gov.cn/zwgk/zfxxgkml/szfwj/qtgw/202206/t20220615_10818266.html (accessed on 10 March 2022).

39. Ministry of Ecology and Environment of the People's Republic of China. *Limits and Measurement Methods for Emissions from Light-Duty Vehicles (CHINA 6) 2016*; Ministry of Ecology and Environment of the People's Republic of China: Beijing, China, 2016.

40. Bureau of Ecology and Environment of Chongqing. 2020 Chongqing Environmental Statistics Annual Report. Available online: http://sthjj.cq.gov.cn/zwgk_249/zfxxgkzl/fdzdgknr/hjtj/202201/t20220124_10332823.html (accessed on 17 June 2022).

41. Bureau of Statistics of Chongqing. Chongqing National Economic and Social Development Statistical Bulletin 2017. Available online: http://tjj.cq.gov.cn/zwgk_233/fdzdgknr/tjxx/sjzl_55471/tjgb_55472/202002/t20200219_5274429.html (accessed on 18 July 2022).

42. Wong, Y.J.; Shiu, H.-Y.; Chang, J.H.-H.; Ooi, M.C.G.; Li, H.-H.; Homma, R.; Shimizu, Y.; Chiueh, P.-T.; Maneechot, L.; Nik Sulaiman, N.M. Spatiotemporal Impact of COVID-19 on Taiwan Air Quality in the Absence of a Lockdown: Influence of Urban Public Transportation Use and Meteorological Conditions. *J. Clean. Prod.* **2022**, *365*, 132893. [CrossRef] [PubMed]

43. Su, Y.; Liu, X.; Li, X. Research on Traffic Congestion Based on System Dynamics: The Case of Chongqing, China. *Complexity* **2020**, *2020*, e6123896. [CrossRef]

44. Chongqing Commission of Housing and Urban-Rural Development. *The 14th Five-Year Plan for Urban Rail Transit Construction in Chongqing (2021–2025) 2022*; Chongqing Commission of Housing and Urban-Rural Development: Chongqing, China, 2022.

45. Tan, R.; Tang, D.; Lin, B. Policy Impact of New Energy Vehicles Promotion on Air Quality in Chinese Cities. *Energy Policy* **2018**, *118*, 33–40. [CrossRef]

46. Chongqing Energy Bureau; Chongqing Development and Reform Commission. *"14th Five-Year" Development Plan for Charging Infrastructure in Chongqing (2021–2025) 2022*; Chongqing Commission of Housing and Urban-Rural Development: Chongqing, China, 2022.

47. Li, L.; Li, Z.-L.; Zhang, D.; Fang, W.-K.; Xu, Q.; Duan, L.-F.; Lu, P.-L.; Wang, F.-W.; Zhang, W.-D.; Zhai, C.-Z. Pollution Characteristics and Source Apportionment of Atmospheric VOCs During Ozone Pollution Period in the Main Urban Area of Chongqing. *Huan Jing Ke Xue Huanjing Kexue* **2021**, *42*, 3595–3603. [CrossRef]

48. Tian, J.; Fang, C.; Qiu, J.; Wang, J. Analysis of Ozone Pollution Characteristics and Influencing Factors in Northeast Economic Cooperation Region, China. *Atmosphere* **2021**, *12*, 843. [CrossRef]

49. Liu, Y.; Zhou, Y.; Lu, J. Exploring the Relationship between Air Pollution and Meteorological Conditions in China under Environmental Governance. *Sci. Rep.* **2020**, *10*, 14518. [CrossRef]

50. Chen, Y.; Zhang, S.; Peng, C.; Shi, G.; Tian, M.; Huang, R.-J.; Guo, D.; Wang, H.; Yao, X.; Yang, F. Impact of the COVID-19 Pandemic and Control Measures on Air Quality and Aerosol Light Absorption in Southwestern China. *Sci. Total Environ.* **2020**, *749*, 141419. [CrossRef]

51. Borck, R.; Schrauth, P. Population Density and Urban Air Quality. *Reg. Sci. Urban Econ.* **2021**, *86*, 103596. [CrossRef]

52. Lin, B.; Zhu, J. Changes in Urban Air Quality during Urbanization in China. *J. Clean. Prod.* **2018**, *188*, 312–321. [CrossRef]

53. Bureau of Quality and Technical Supervision of Hubei. *Specification Requirements of Construction and Acceptance for Hubei Province Ambient Air Quality Automatic Monitoring System 2011*; Bureau of Quality and Technical Supervision of Hubei: Wuhan, China, 2011.

54. Yao, Q.; Kwok, J.T.; Wang, T.; Liu, T.-Y. Large-Scale Low-Rank Matrix Learning with Nonconvex Regularizers. *IEEE Trans. Pattern Anal. Mach. Intell.* **2019**, *41*, 2628–2643. [CrossRef]

55. Candes, E.J.; Tao, T. The Power of Convex Relaxation: Near-Optimal Matrix Completion. *IEEE Trans. Inf. Theory* **2010**, *56*, 2053–2080. [CrossRef]

56. Tan, S.; Wang, Y.; Yuan, Q.; Zheng, L.; Li, T.; Shen, H.; Zhang, L. Reconstructing Global $PM_{2.5}$ Monitoring Dataset from OpenAQ Using a Two-Step Spatio-Temporal Model Based on SES-IDW and LSTM. *Environ. Res. Lett.* **2022**, *17*, 034014. [CrossRef]

57. Noor, M.N.; Yahaya, A.S.; Ramli, N.A.; Al Bakri Abdullah, M.M. Filling the Missing Data of Air Pollutant Concentration Using Single Imputation Methods. *Appl. Mech. Mater.* **2015**, *754–755*, 923–932.

58. Chen, L.; Jiang, X.; Liu, X.; Zhou, Z. Logarithmic Norm Regularized Low-Rank Factorization for Matrix and Tensor Completion. *IEEE Trans. Image Process.* **2021**, *30*, 3434–3449. [CrossRef]